

Fast Flat Fields from Scanning Extended Sources

N. E. DALRYMPLE,¹ M. BIANDA,² AND P. H. WIBORG¹

Received 2002 December 12; accepted 2003 February 10

ABSTRACT. A fast flat-fielding algorithm is presented that uses two orthogonal constant-speed scans of an image across a detector to compute a flat field. Each scan image calibrates the cross-scan direction of the other. Results from the ISOON solar telescope are presented. For a camera with 2048×2048 pixels, the computation requires 30 s of processing time and yields a result that is comparable to a Kuhn-Lin flat field, which requires 1 hr of processing time on the same system. The total system photometric accuracy using the fast method is about 1%. The method has been tested for full-disk and high-resolution solar imaging.

1. INTRODUCTION

The Air Force Improved Solar Optical Observing Network (ISOON) is an automated patrol telescope that uses a tunable Fabry-Perot filter system to image the full solar disk in multiple wavelengths at rapid cadence. Because of the variety of wavelengths and the thermal sensitivity of the Fabry-Perot filter system, the capability to rapidly acquire and compute image correction tables, or flat fields, is essential to the successful operation of ISOON. Approximately 22 optical surfaces lie near focus, and these surfaces introduce much of the nonuniform optical response that requires flat-field correction. Simply throwing the telescope out of focus changes the optical response, so this method of obtaining flat fields cannot be used. Sky flats (Chromey & Hasselbacher 1996) are not acceptable because of the large intensity gradients near the Sun, and dome flats require the mechanical complexity of adding a flip-in dome to the ISOON optical train. Kuhn, Lin, & Lorz (1991) and Wild (1997) present methods of flat-fielding using only image data, and the first ISOON flat fields were computed using the algorithm of Kuhn et al. (1991). While the resulting flat fields had acceptable quality, they required approximately 1 hr to compute on the ISOON system. The present flat-fielding algorithm was developed in an effort to reduce the computation time. The ISOON flat-field code now runs in about 30 s.

The inspiration for the faster algorithm came from wearing smudged spectacles and noting that one unconsciously corrects visual images by observing an extended object and scanning with one's head. Details that do not appear to move with the observed object are interpreted as optical imperfections. In the same manner, the relative pixel gains of a CCD camera observing through an optical system can be calculated. The result is a flat-field table that is used repeatedly to correct subsequent

images. In a typical observation sequence, the observing system is off-pointed to an appropriate starting position. The exposure is then begun and the system is linearly scanned across the source. At the end of the scan, the exposure is terminated. The process is repeated for the orthogonal scan direction, yielding two scan images. Section 2 describes how these two images are used to determine the system flat field, and a practical implementation is outlined in § 3. Error sources are discussed in § 4, and § 5 presents some ISOON results. A portion of the ISOON flat-fielding code is located in the Appendix.

2. THEORY

Consider a generic imaging system where light from a source passes through some optical system and is detected at a measurement surface. We define the flat field f to be the ratio of the measured intensity m to the intensity that would be measured by a perfect sensor and optical system p :

$$f(\mathbf{r}, t) = \frac{m(\mathbf{r}, t)}{p(\mathbf{r}, t)}. \quad (1)$$

Here \mathbf{r} is the two-dimensional detector position vector and t is time. Throughout this section, it is assumed that dark current has been subtracted from measured images. Neither f nor p is known. The challenge is to determine f using only image data. Once f is determined, corrected images are calculated using $p = m/f$. If f does not vary in time, the recorded image M is the time integral over the exposure E :

$$M(\mathbf{r}) = f(\mathbf{r}) \int_0^E p(\mathbf{r}, t) dt. \quad (2)$$

Now consider a time-invariant light source that is scanned relative to the field of view along some path C , defined by $\mathbf{r}_0(t)$ (see Fig. 1). In this case, the time dependence of p is

¹ Air Force Research Laboratory, Space Vehicles Directorate, National Solar Observatory, Sunspot, NM 88349; dalryn@nso.edu, kcjones@nso.edu.

² Istituto Ricerche Solari Locarno (IRSOL), CH-6605 Locarno-Monti, Switzerland; mbianda@irsol.ch.

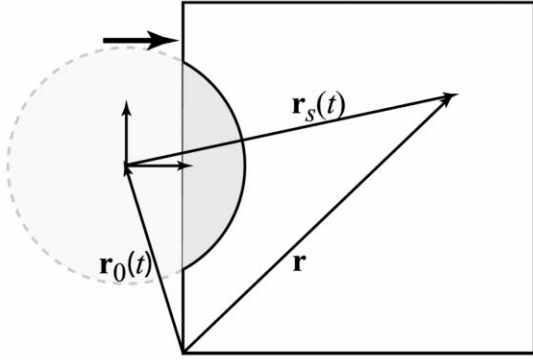


FIG. 1.—Scan geometry, showing coordinate systems.

entirely the result of the motion of the source. That is,

$$p(\mathbf{r}, t) = s[\mathbf{r}_s(t)] = s[\mathbf{r} - \mathbf{r}_0(t)], \quad (3)$$

where $s(\mathbf{r}_s)$ is the time-invariant source, $\mathbf{r}_s \equiv$ coordinates with respect to the source, $\mathbf{r} \equiv$ CCD coordinates, and $\mathbf{r}_0 \equiv$ CCD coordinates of the source origin. Equation (2) becomes

$$M(\mathbf{r}) = f(\mathbf{r}) \int_0^E s[\mathbf{r} - \mathbf{r}_0(t)] dt. \quad (4)$$

If C does not cross itself, and the movement does not stop during the exposure, then \mathbf{r}_0 is a one-to-one function of t . Regarding $t = t(\mathbf{r}_0)$, equation (4) can be converted to a line integral:

$$M(\mathbf{r}) = f(\mathbf{r}) \int_C s(\mathbf{r} - \mathbf{r}_0) \nabla t \cdot d\mathbf{r}_0. \quad (5)$$

The integral in equation (5) averages s along C , weighted by the velocity profile. If the scan velocity is constant and linear, uniform illumination is provided *in a time-averaged sense* along paths parallel to C .

Specifying to the case of a linear scan at constant velocity, let $\mathbf{r} = x\mathbf{x} + y\mathbf{y}$, where \mathbf{x} and \mathbf{y} are orthogonal unit vectors aligned with convenient scan directions (altitude and azimuth, right ascension and declination, etc.). Scanning in x , with $\mathbf{r}_0(t) = x_0(t)\mathbf{x} + y_0\mathbf{y}$, $x_0(t) = x_1 + v_x t$, and y_0 constant gives

$$M_x(x, y) = \frac{f(x, y)}{v_x} \int_{x_1}^{x_1 + v_x E} s(x - x_0, y - y_0) dx_0. \quad (6)$$

The integral in equation (6) is, to within a constant, the spatial average of s along x over the source coordinate interval $[x - x_1, x - (x_1 + v_x E)]$, denoted $\bar{s}_x(x, y - y_0)$. Equation

(6) may be solved for the flat field:

$$f(x, y) = \frac{M_x(x, y)}{E\bar{s}_x(x, y - y_0)}. \quad (7)$$

For some sources, \bar{s}_x may be approximated as constant in x (see § 4). That is, the average is weakly dependent upon the interval over which the average is taken. In these cases, an x -scan image M_x fixes f to within a function of y ,

$$f(x, y) = b(y)M_x(x, y). \quad (8)$$

Similarly, a y -scan image M_y fixes f to within a function of x :

$$f(x, y) = a(x)M_y(x, y). \quad (9)$$

Figure 2 shows examples of M_x and M_y obtained with the ISOON telescope.

Since the f in equations (8) and (9) must be equal, the a and b are related. Choosing $y = y_1$,

$$\begin{aligned} f(x_1, y_1) &= a(x_1)M_y(x_1, y_1) = b(y_1)M_x(x_1, y_1), \\ f(x_2, y_1) &= a(x_2)M_y(x_2, y_1) = b(y_1)M_x(x_2, y_1), \\ &\vdots \\ f(x_N, y_1) &= a(x_N)M_y(x_N, y_1) = b(y_1)M_x(x_N, y_1). \end{aligned} \quad (10)$$

From this, we see that $a(x) = b(y_1)M_x(x, y_1)/M_y(x, y_1)$, which can be substituted into equation (9) to yield

$$f_1(x, y) = b(y_1) \frac{M_x(x, y_1)}{M_y(x, y_1)} M_y(x, y), \quad (11)$$

where the subscript “1” in $f_1(x, y)$ refers to the arbitrary choice of $y = y_1$ as the normalizing chord for this exercise.

Any horizontal slice j will give a similar estimate of f :

$$f_j(x, y) = b(y_j) \frac{M_x(x, y_j)}{M_y(x, y_j)} M_y(x, y). \quad (12)$$

The estimates f_j can be combined in a suitable average to give a more robust flat field. One approach is to set all the constants $b(y_j) = 1$. Alternatively, each f_j can be normalized to a mean magnitude of unity before combining. The averaging process for the first case is given by

$$\begin{aligned} \bar{f}_y(x, y) &= \frac{1}{N_j} \sum_j f_j(x, y) \\ &= \frac{M_y(x, y)}{N_j} \sum_j \frac{M_x(x, y_j)}{M_y(x, y_j)}, \end{aligned} \quad (13)$$

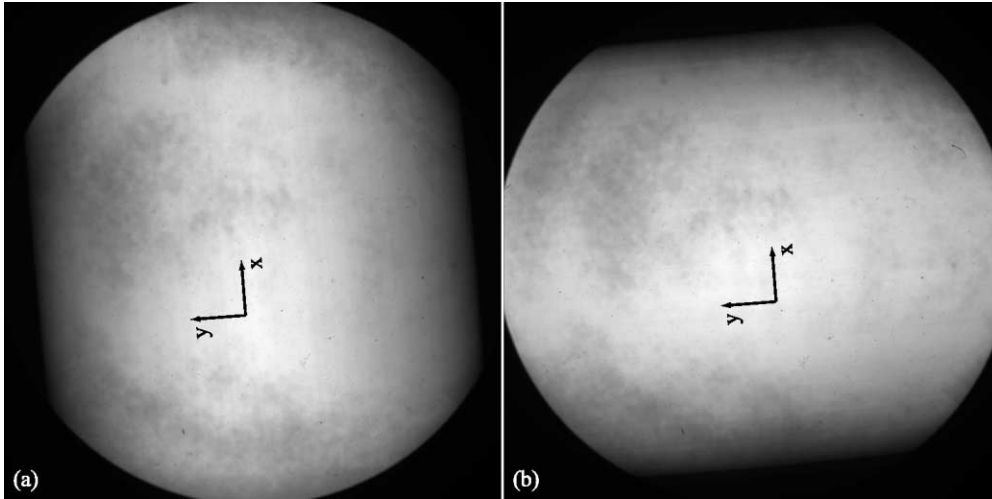


FIG. 2.—Raw ISOON scan images observed on 2002 September 26, using the full solar disk as a light source. (a) R.A. scan, M_x ; (b) decl. scan, M_y . Arrows show the approximate directions of x and y .

where the subscript y on \bar{f}_y indicates that the flat-field estimate is based upon a y -scan image whose columns have been normalized.

The choice of x and y axes is arbitrary, so equation (13) holds also in the other direction:

$$\begin{aligned}\bar{f}_x(x, y) &= \frac{1}{N_i} \sum_i f_i(x, y) \\ &= \frac{M_x(x, y)}{N_i} \sum_i \frac{M_y(x_i, y)}{M_x(x_i, y)}.\end{aligned}\quad (14)$$

Here the subscript x on \bar{f}_x indicates that the flat-field estimate is based upon an x -scan image whose rows have been normalized. Equations (13) and (14) are two separate estimates of the flat field.

In summary, for sources and scan arrangements such that \bar{s}_x is independent of x , each scanwise chord through a scan image i is the flat field *along that particular chord*. The scale factors of adjacent chords cannot be determined from a single image, since the particular source viewed during the scan is unknown. However, a single chord from a second orthogonal scan image fixes the scaling of every chord of the first image that it crosses. Each cross-cutting chord gives a separate flat-field estimate. A large number of estimates may be averaged to give a very robust flat field.

3. ISOON IMPLEMENTATION

At this point, it is helpful to outline the practical implementation of the fast flat-field algorithm. Scan images M_x and M_y are measured as the ISOON telescope scans in right ascension (R.A.) and declination (decl.), respectively (see Fig. 2). The scans start with the solar disk completely outside the detector, con-

tinue across the Sun at constant velocity, and end with the solar disk completely outside the detector on the opposite side. Following image acquisition, the CCD dark current is subtracted and the images are rotated so that the R.A. and decl. scan directions are aligned with the vertical and horizontal axes. Flat fields are computed in IDL (see code in Appendix) and then rotated back into proper orientation with the camera.

During full-disk observations, ISOON's field of view (2.3 solar radii) is larger than the solar diameter. Scanning the Sun across the CCD only partially illuminates the chip. Noisy regions appear in \bar{f}_x at the top and bottom where the illumination is relatively small (Fig. 3a). Similarly, \bar{f}_y contains noisy regions at the left and right (Fig. 3b). A composite flat field is assembled from pieces of \bar{f}_x and \bar{f}_y in such a way that the noisy regions are eliminated. First, \bar{f}_x is normalized, taking only the central area where there is significant overlap in the calculation of the norm. Once normalized, pieces of \bar{f}_x can be used to "patch" the poorly illuminated portions of \bar{f}_y . Four small areas at the corners of the image are left without a flat-field table, but these areas lie outside the telescope aperture. Despite its inelegance, this approach works satisfactorily in the ISOON system. High-resolution ISOON observations have a smaller field of view, and mating flat fields is not required.

4. ERROR SOURCES

In writing equation (8), we have assumed that the average of s along x is independent of the particular interval over which the average is taken. The validity of this assumption depends upon the particular source used and the scanning arrangement. If a pixel at CCD position $x = 0$ is scanned over the interval $[x_1, x_2]$, the pixel located at CCD position $x = W$ will be scanned over $[x_1 + W, x_2 + W]$. In general, \bar{s}_x will change across the CCD as a result of averaging over different intervals. In

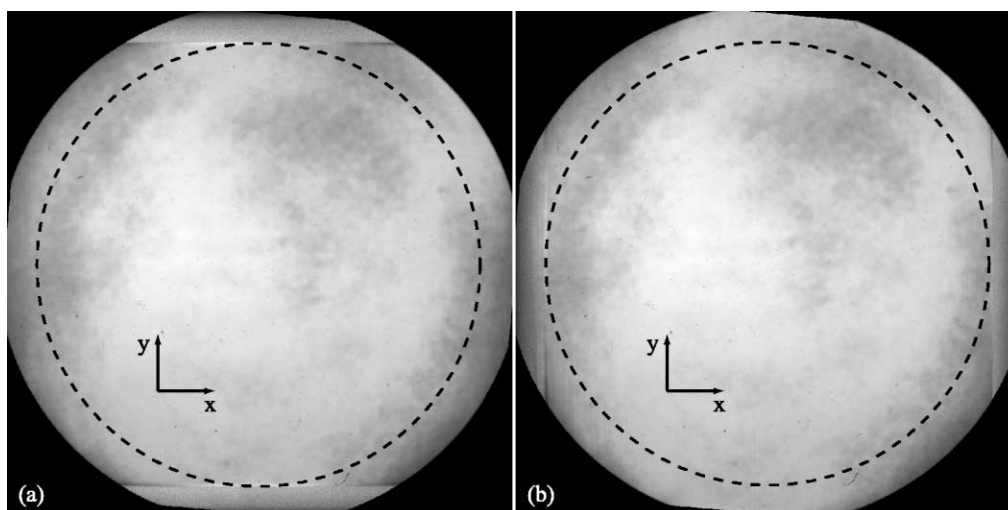


FIG. 3.—Individual flat fields before mating, computed using M_x and M_y of Fig. 2. (a) \bar{f}_x from eq. (14); (b) \bar{f}_y from eq. (13). The solar disk (*dashed circle*) is smaller than the field of view, so that portions of the detector at the top and bottom in *a* and at left and right in *b* are poorly illuminated. The two flat-field estimates are very similar in the central region, where both are well illuminated. Areas outside the aperture appear dark. Arrows show the approximate directions of x and y .

solar observations, the disk of the Sun is much brighter than the surrounding sky. The ISOON scans begin with the solar disk completely outside the detector and finish with the disk completely outside the detector on the opposite side. Neglecting illumination by the sky, every pixel in a line along the scan direction sees the same time-integrated illumination. Scans that only partially traverse the solar disk introduce a secular variation in \bar{s}_x due to limb darkening that shows up in the final flat field as a large-scale gradient.

Although this algorithm has not been tested in nighttime

applications, we offer two strategies for obtaining an x -independent \bar{s}_x . First of all, one could use the Moon or a planetary disk as an illumination source, in the same manner that ISOON uses the Sun. This would require a viewable disk and the ability to repoint between flat-field acquisitions. A second strategy is to perform scans over swaths of sky that extend sufficiently far to reduce the x -variation in \bar{s}_x below acceptable levels. For sparse, high-contrast sources, this may not be realistic, limiting the usefulness of this algorithm.

The two image rotations used to align the scan directions

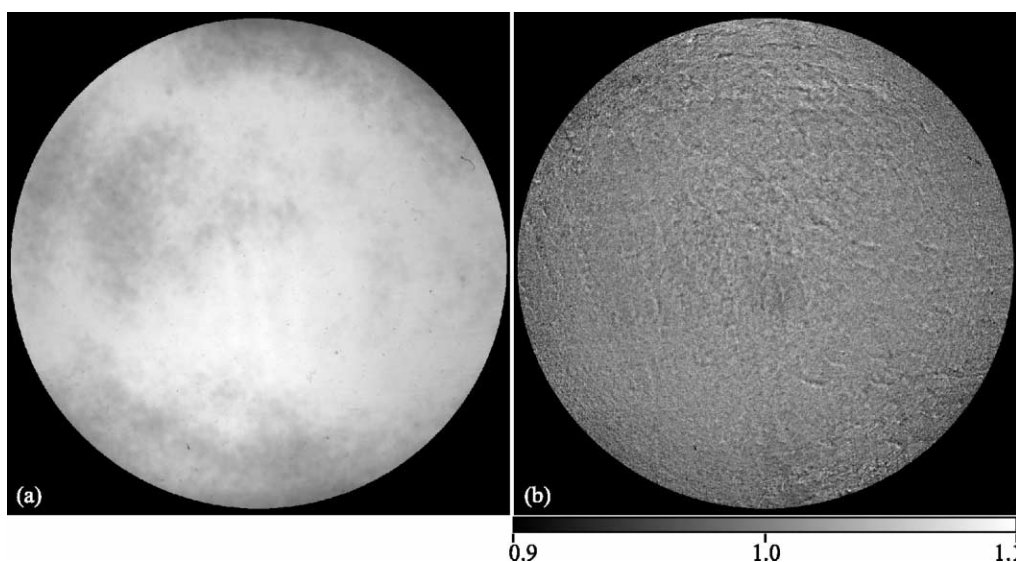


FIG. 4.—(a) Composite flat field computed using the algorithm of the present paper; (b) ratio of flat field to Kuhn-Lin flat field (Kuhn et al. 1991). Data obtained within 5 minutes. A plane has been removed. Color scaled to $\pm 10\%$.

with the detector axes introduce resampling errors. In the ISOON system, these are unavoidable but negligible. Accurate alignment of the scan directions with the rows and columns of the detector would make the two resampling steps unnecessary.

Another error source arises because scans in declination do not produce perfectly linear scans across the detector, but introduce some image rotation during the scan. This effect is quite small—unnoticeable in the ISOON system.

During development of the present algorithm, several other factors specific to the ISOON instrument have been noted and corrected. Scanning completely over the Sun in continuum exceeds the dynamic range of the detector, so a neutral density (ND) filter was installed in the aperture plane. Flat-field scans are now viewed through the ND filter, which is moved aside for still exposures. Over large scales, the small difference in optical path length is not noticeable, but at scales of order the pixel size a slight change in image scale is observed. This is hoped to be solved by faster scanning, obviating the need for the ND filter, or by insertion of an identical thickness of antireflection-coated glass (ND 0) during still exposures. Instrumental scattered light can vary over the range of pointing angles and is remedied by precise alignment of optics and internal baffling. The telescope scan velocity was initially non-constant and had to be corrected. Synchronizing the scan start and shutter trigger improved the flat-field quality. The Sun itself is time-variant during the initial stages of bright flares. Flat-fielding during these rapid solar events sometimes yields streaks in the computed flat field. Finally, truly opaque optical imperfections, such as dirt or insects, give $f = 0$ and are not completely corrected.

5. ISOON RESULTS

The composite flat-field solution computed using M_x and M_y of Figure 2 is shown in Figure 4a. To test the accuracy of

the solution, Figure 4b shows the ratio of the flat field in Figure 4a to a flat field for the same time period computed using the established method of Kuhn et al. (1991). The color scale has been expanded to span the range from 0.9 to 1.1 (or $\pm 10\%$). The two solutions differ by a plane, which has been removed. As noted in Kuhn et al. (1991), for an infinite pixel domain with no gaps, the Kuhn-Lin gain solution contains a gradient ambiguity. Examination of solar-image data indeed reveals a brightness gradient in ISOON images processed using the Kuhn-Lin algorithm. It is possible that more iteration would remove this ambiguity. Apart from the gradient, the standard deviation of the ratio of the two flat-field solutions is 2.0%. Deviations from the Kuhn-Lin solution appear as sets of shifted features that resemble solar filaments and convection cells. Close examination reveals that these features are visible in the Kuhn-Lin flat field but not in the fast flat field. We believe that these are in fact “bleed-through” solar features resulting from too few images in the Kuhn-Lin observation set. We used 17 images to compute the Kuhn-Lin flat field, and it is possible that a larger number of images would reduce this effect.

In a second test of the accuracy of the fast method, images were recorded in quick succession at several ISOON point directions, shifted by some $10'$. The images were each reduced using the same flat field. This procedure imaged the same solar features through different portions of the aperture. The intensities of corresponding solar features were then compared, yielding a total system photometric accuracy of about 1%.

Table 1 compares the computational performance of the present algorithm to the method of Kuhn et al. (1991). Run time of the present algorithm is faster by 2 orders of magnitude, and memory usage is down by a factor of 2.7. In addition to performance gains, the scanning algorithm does not require accurate position information. This has the effect of increased robustness in changing atmospheric conditions (clouds) and

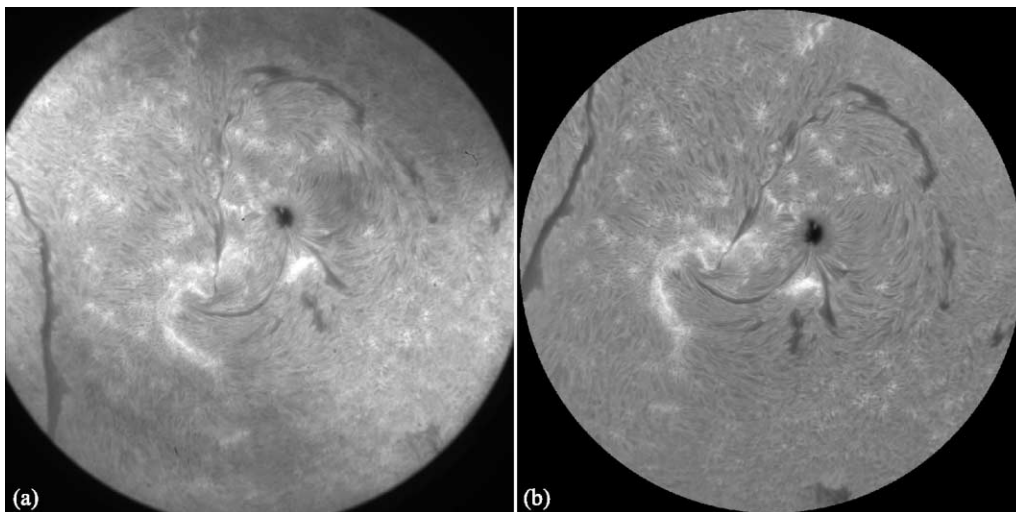


FIG. 5.—High-resolution solar observations: (a) Raw image; (b) corrected and rotated image.

TABLE 1
PERFORMANCE COMPARISON OF FLAT-FIELD ALGORITHMS

Metric	Present Algorithm	Kuhn et al. 1991
Number of images	2	17 or more
Implementation	All IDL	IDL and C
Memory usage (MBytes)	68.9	185
Run time (s)	28.5	2933
Plane ambiguity	No	Yes
Position required	No	Yes

NOTE.—Performance tested on a Sun Blade 100 workstation with 384 MBytes RAM running SunOS 5.8.

allows the method to be used for high-resolution solar observations and other extended source imaging without correlation tracking.

The fast flat-field algorithm may be used without modification for sources other than the full solar disk. Figure 5 shows raw and corrected high-resolution solar images with a field of view of approximately $10'$. The uncorrected ISOON images contain many flaws of both large and small scale. These are the result of the large number of optical surfaces near focus and of the relative passband mismatch between the two Fabry-Perot filters. Those features due to the Fabry-Perot etalons change on a 30 minute timescale as a result of small thermal

variations. The ISOON optical system thus represents a kind of worst-case flat field.

6. CONCLUSIONS

A fast flat-fielding algorithm has been developed that uses two images to compute a flat field. During each exposure, an extended source is scanned across the field of view. For the case of the ISOON system, the computation requires about 30 s and yields a result comparable to a Kuhn-Lin flat field, which requires 17 images and 3000 s of processing time on the same system. The total system photometric accuracy using the fast method is about 1%. The method applies in cases where the intensity of the observed source changes slowly with respect to the camera exposure time, where the optical configuration remains constant during the scans, and where the path of motion is known or can be deduced from the images. The speed of the algorithm makes this flat-fielding method attractive for use when computational and image acquisition time is limited.

We gratefully acknowledge the contributions of Diane Craig, Dick Dunn, Craig Gullixson, Bill Hull, Joel Mozer, Don Neidig, Jan Richards, and Neil Snyder. This work was supported by the Air Force Office of Scientific Research.

APPENDIX

ISOON FAST FLAT FIELDING CODE

The following is the IDL code that implements the fast flat fielding algorithm in the ISOON system. `Mdec` and `Mha` are the M_y and M_x from above and `amask` is an aperture mask byte array. In this function, the images `Mdec` and `Mha` are assumed to be dark-corrected and rotated so that the scan directions line up with the rows and columns. The ISOON system averages only the middle half of the cross-cutting chords, where the solar-disk light is brightest.

```
function mflat_make_flat, Mdec, Mha, amask
; set defaults
if (N_Elements (amask) eq 0) then amask = 1b

; limit images to > 1
Mdec = Temporary(Mdec) > 1
Mha = Temporary(Mha) > 1
; compute array sizes
s = Size (Mdec)
sx = s[1] & sy = s[2]

; Use middle 1/2 of data for calculation
; first, compute the dec-dir flat
fdec = Mdec*(Total(Mha[* ,sy/4:3*sy/4])/Float(Mdec[* ,sy/4:3*sy/4]),2) # Replicate(1, sy))/Float(sy)*amask

; then compute the ha-dir flat
fha = Mha*(Total(Mdec[sx/4:3*sx/4,*])/Float(Mha[sx/4:3*sx/4,*]), 1) ## Replicate(1, sx))/Float(sx)*amask
```

```

; optional: clear image matrices to conserve memory
Mdec = 0b & Mha = 0b

; Mate two flat field estimates together
; Compute norms using middle 500x500 patch
x1 = sx/2-250 & x2 = x1+500
y1 = sy/2-250 & y2 = y1+500
hod = float(Mean(fha[x1:x2,y1:y2]/Double(fdec[x1:x2,y1:y2])))

; Replace the first and last 1/5
mask = Replicate(0b, sx)
mask[sx/5:4*sx/5] = 1b
mask = mask # Replicate(1b, sy)
fdec = Temporary(fdec)*mask + Temporary(fha)/hod*(1b-mask)

; Normalize flat so that the mean is 1
norm = Mean(fdec[sx/4:3*sx/4, sy/4:3*sy/4])
fdec = Temporary(fdec)/norm

; fdec is now a composite of fdec and fha
return, fdec
end

```

REFERENCES

- Chromey, F. R., & Hasselbacher, D. A. 1996, *PASP*, 108, 944
 Kuhn, J. R., Lin, H., & Lorz, D. 1991, *PASP*, 103, 1097
 Wild, W. J. 1997, *PASP*, 109, 1269